Replies to comments of Editor

Authors would like to express sincere gratitude to the Editor for his constructive comments. Our manuscript has greatly benefited from these insights. We have carefully revised the manuscript, taking the given comments into account. Our responses to the editor's comments are provided below.

(1) Please present a theoretical figure of the slope Eq. (1) against wavelengths and/or SZA to indicate the method is consistent with the principle of the atmospheric radiative transfer theory. It is OK to make a simple radiative transfer calculation with plane parallel models of aerosol and cloud laden atmospheres. Such a theoretical computation will contribute to answering some reviewers' comments.

→ We sincerely thank the Editor for this valuable and insightful comment. In response, we have substantially revised the methodology and made corresponding revisions throughout the manuscript. In addition, we performed radiative-transfer simulations and incorporated the results into the revised manuscript to clarify the physical mechanism underlying the proposed cloud-screening method. First, we revised the methodology as follows:

For the zenith sky radiance signals $S(\lambda_1)$ and $S(\lambda_2)$ observed at any two wavelengths λ_1 and λ_2, the slope value (m_{obs}) can be expressed using the following equation:

$$m_{obs}(\lambda_1,\lambda_2) = \frac{\ln[S(\lambda_1)/S(\lambda_2)]}{\ln(\lambda_1/\lambda_2)}. \qquad \text{(R1)}$$

The measured zenith sky radiance can be further represented as

$$S(\lambda) = C(\lambda)L(\lambda), \qquad \text{(R2)}$$

where $L(\lambda)$ is the band-averaged atmospheric zenith radiance and $C(\lambda)$ is the wavelength-dependent relative instrumental response. Substituting Eq. (2) into Eq. (1), we can write

$$m_{obs}(\lambda_1,\lambda_2) = \frac{\ln[\frac{C(\lambda_1)L(\lambda_1)}{C(\lambda_2)L(\lambda_2)}]}{\ln(\lambda_1/\lambda_2)} \qquad \text{(R3)}$$

Using ln(ab) = ln(a) + ln(b),

$$m_{obs}(\lambda_1,\lambda_2) = \frac{\ln[\frac{C(\lambda_1)}{C(\lambda_2)}]}{\ln(\lambda_1/\lambda_2)} + \frac{\ln[\frac{L(\lambda_1)}{L(\lambda_2)}]}{\ln(\lambda_1/\lambda_2)}. \qquad \text{(R4)}$$

Thus,

$$m_{obs}(\lambda_1,\lambda_2) = m_{atm}(\lambda_1,\lambda_2) + m_{inst}(\lambda_1,\lambda_2), \qquad \text{(R5)}$$

where,

$$m_{atm}(\lambda_1,\lambda_2) = \frac{\ln[\frac{L(\lambda_1)}{L(\lambda_2)}]}{\ln(\lambda_1/\lambda_2)}, \qquad \text{(R6)}$$

and

$$m_{inst}(\lambda_1, \lambda_2) = \frac{\ln\left[\frac{C(\lambda_1)}{C(\lambda_2)}\right]}{\ln(\lambda_1/\lambda_2)}. \qquad \text{(R7)}$$

Similary, the extra-terrestrial instrument signal F_0 (i.,e calibration constant) at wavelength λ can be expressed as

$$F_0(\lambda) = C(\lambda)E_0(\lambda), \qquad \text{(R8)}$$

where $E_0(\lambda)$ is band-averaged extra-terresital solar irradiance at wavelenght λ. For the two wavelengths λ_1 and λ_2,

$$\frac{C(\lambda_1)}{C(\lambda_2)} = \frac{F_0(\lambda_1)}{F_0(\lambda_2)}\frac{E_0(\lambda_2)}{E_0(\lambda_1)} \qquad \text{(R9)}$$

Consequntly, from Eqs. (7) and (9),

$$m_{inst}(\lambda_1, \lambda_2) = \frac{\ln[\frac{F_0(\lambda_1)}{F_0(\lambda_2)}\frac{E_0(\lambda_2)}{E_0(\lambda_1)}]}{\ln(\lambda_1/\lambda_2)}. \qquad \text{(R10)}$$

Since $m_{atm}(\lambda_1, \lambda_2) = m_{obs}(\lambda_1, \lambda_2) - m_{inst}(\lambda_1, \lambda_2)$, from Eqs. (5), and (10) we can write,

$$m_{atm}(\lambda_1, \lambda_2) = \frac{\ln[S(\lambda_1)/S(\lambda_2)]}{\ln(\lambda_1/\lambda_2)} - \frac{\ln[\frac{F_0(\lambda_1)E_0(\lambda_2)}{F_0(\lambda_2)E_0(\lambda_1)}]}{\ln(\lambda_1/\lambda_2)} \qquad \text{(R11)}$$

represents the contribution arising from the wavelength-dependent relative response of the instrument.
Here, m_{atm} represents the atmospheric contribution arising from molecular, aerosol, and cloud scattering together with atmospheric absorption, and m_{inst} represents the wavelength-dependent instrumental contribution. To calculate m_{atm}, $F_0(\lambda)$ and $E(\lambda)$ are also required along with instrument-observed $S(\lambda)$ values. In this study, $F_0(\lambda)$ values determined from the Improved Langely method and $E_0(\lambda)$ values estimated by integrating the extraterrestrial solar spectrum of Gueymard (2004) over the spectral response function of each sky-radiometer channel were used. The resulting correction should be regarded as a first-order estimate of the wavelength-dependent instrumental contribution, because a single set of median spectral calibration constants was applied to each instrument over the corresponding analysis period. Nevertheless, a key advantage of this approach is that, even with such a first-order approximation, the corrected atmospheric spectral slope, m_{atm}, retains sufficient sensitivity to distinguish between cloud-free and cloud-contaminated conditions, as demonstrated and discussed in the Results and Discussion in the revised manuscript.

To explain the physical mechanism underlying the proposed method, we performed plane-parallel radiative-transfer simulations using the Santa Barbara DISORT Atmospheric Radiative Transfer (SBDART) model (Ricchiazzi et al., 1998) at wavelengths of 0.380, 0.400, 0.500, 0.675, 0.870, and 1.020 µm. The simulations were conducted over a range of solar zenith angles (SZAs) for four representative atmospheric conditions: (1) a clean cloud-free atmosphere with an aerosol optical thickness at 0.55 µm (AOT_{550}) of 0.10; (2) a polluted cloud-free atmosphere with AOT_{550} = 0.50; (3) a thin-cloud atmosphere with AOT_{550} = 0.10 and cloud optical thickness at 0.55 µm (COT_{550}) = 2; and (4) a thick-cloud atmosphere with AOT_{550} = 0.10 and COT_{550} = 20. The simulations assumed a mid-latitude summer atmospheric profile, precipitable water vapor of 1.0 cm, total column ozone of 0.30 cm-atm, and a Lambertian surface albedo of 0.10, with clouds represented as plane-parallel layers.

For the radiative-transfer simulations, the wavelength-dependent instrumental response was set to unity, i.e., and $C(\lambda) = 1$, and hence $(C(\lambda_1) = C(\lambda_2) = 1)$ for each wavelength pair. Thus, no wavelength-dependent instrumental contribution was included in the simulated radiances, and the spectral slopes calculated from these radiances represent the atmospheric contribution, m_{atm}, directly.

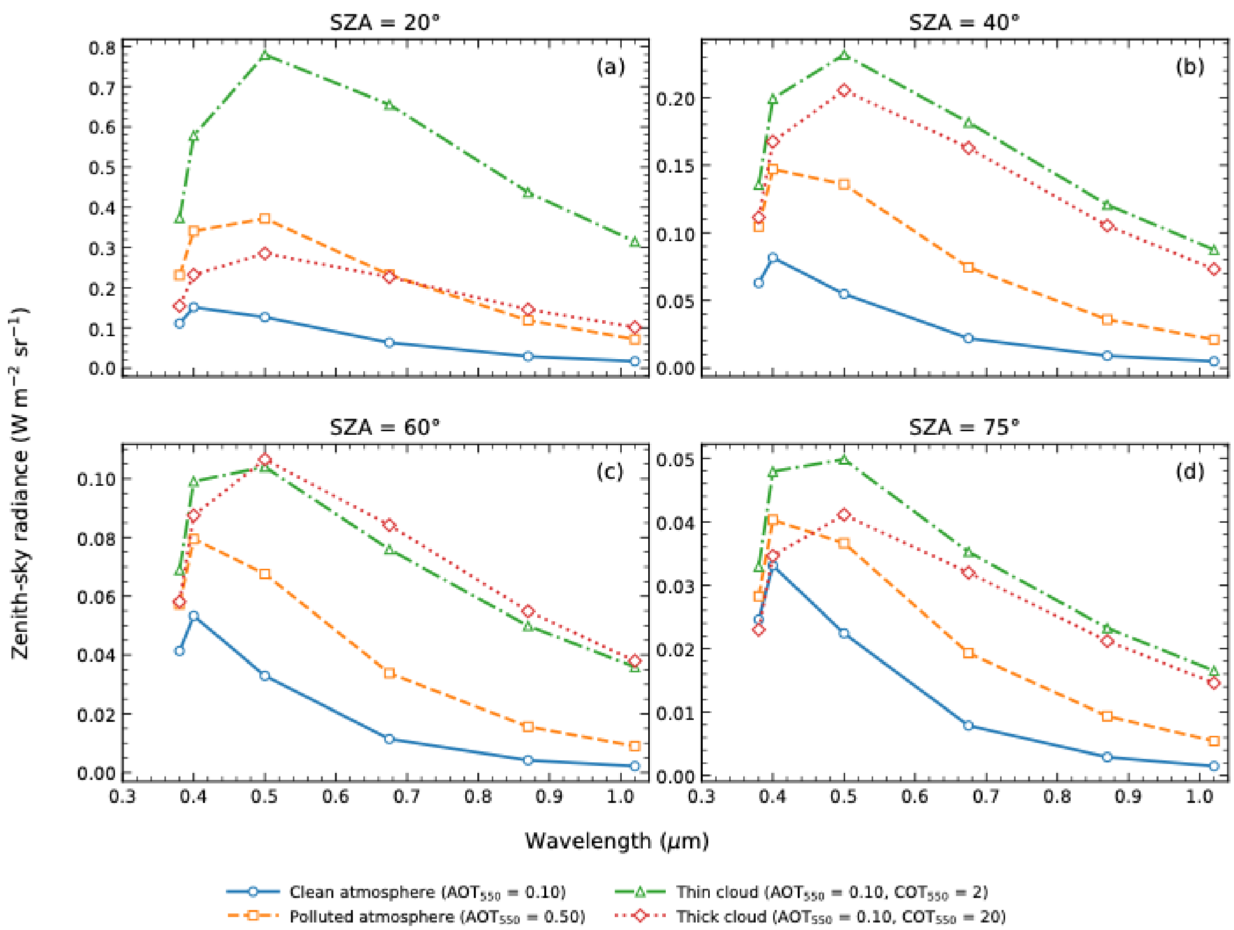

Figure R1. Zenith-sky radiance spectra computed using the SBDART radiative transfer model for solar zenith angles (SZAs) of (a) 20°, (b) 40°, (c) 60°, and (d) 75 for four representative atmospheric conditions: a clean cloud-free atmosphere with an aerosol optical thickness at 0.55 µm (AOT_{550}) of 0.10, a polluted cloud-free atmosphere with AOT_{550} = 0.50, a thin-cloud atmosphere with AOT_{550} = 0.10 and cloud optical thickness at 0.55 µm (COT_{550}) = 2, and a thick-cloud atmosphere with AOT_{550} = 0.10 and COT_{550} = 20. Simulations were performed with mid-latitude summer atmospheric model, precipitable water vapor of 1.0 cm, total column ozone of 0.30 cm-atm, Labertian surface albedo of 0.10, and clouds represented as plane-parallel layers.

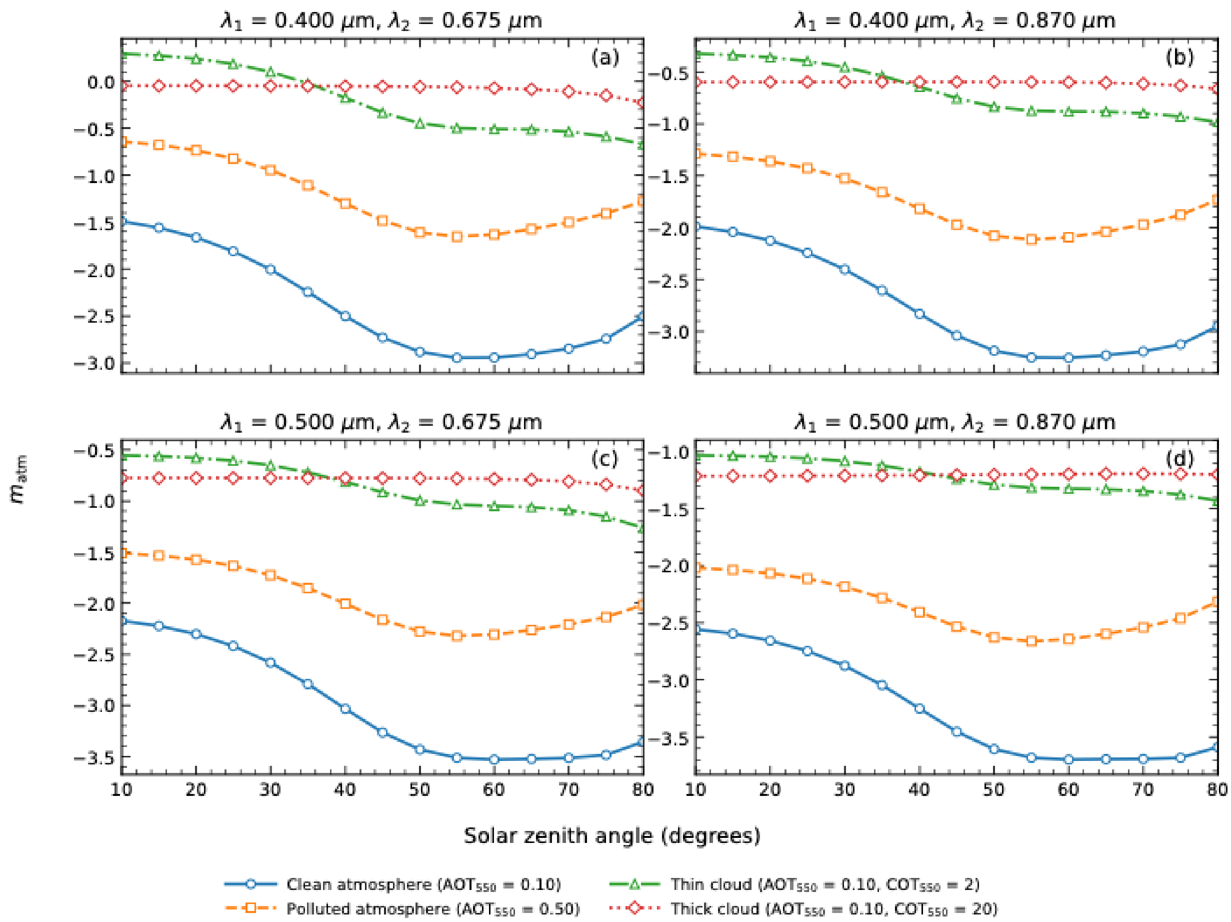

Figure R2. Atmospheric spectral slope (m_{atm}) as a function of solar zenith angle (SZA) simulated for four selected wavelength pairs: (a) 0.400–0.500 µm, (b) 0.400–0.870 µm, (c) 0.500–0.675 µm, and (d) 0.500–0.870 µm for four representative atmospheric conditions: a clean cloud-free atmosphere with an aerosol optical thickness at 0.55 µm (AOT_{550}) of 0.10, a polluted cloud-free atmosphere with AOT_{550} = 0.50, a thin-cloud atmosphere with AOT_{550} = 0.10 and cloud optical thickness at 0.55 µm (COT_{550}) = 2, and a thick-cloud atmosphere with AOT_{550} = 0.10 and COT_{550} = 20. Simulations were performed with mid-latitude summer atmospheric model, precipitable water vapor of 1.0 cm, total column ozone of 0.30 cm-atm, Labertian surface albedo of 0.10, and clouds represented as plane-parallel layers.

Figure R1 presents the simulated zenith-sky radiance spectra for the four representative solar zenith angles (SZAs). Both the magnitude and spectral dependence of the zenith sky radiance vary systematically with atmospheric state and SZA. Under clean cloud-free conditions, the zenith sky radiance generally decreases strongly toward longer wavelengths, primarily reflecting the pronounced wavelength dependence of molecular (Rayleigh) scattering. Increasing aerosol loading modifies both the magnitude and spectral dependence of the radiance because aerosol scattering has a weaker wavelength dependence than Rayleigh scattering. The presence of clouds produces a further substantial modification of the spectral distribution. In particular, cloud scattering tends to flatten the zenith-radiance spectrum, resulting in a considerably weaker wavelength dependence than that observed under clean cloud-free conditions. These simulations therefore demonstrate that cloud-free and cloudy atmospheres produce distinct spectral signatures in zenith-sky radiance, providing a physical basis for using the spectral slope as an indicator of cloud contamination.

To quantify the spectral differences shown in Figure R1, Figure R2 presents m_{atm}, calculated directly from the simulated zenith sky radiances for representative wavelength pairs as a function of SZA. Because $C(\lambda_1) = C(\lambda_2) = 1$ was assumed in these simulations, the calculated spectral slopes represent the atmospheric contribution without any wavelength-dependent instrumental contribution. The clean cloud-free atmosphere generally exhibits the largest negative values of m_{atm}, reflecting the strong decrease in radiance with increasing wavelength associated primarily with Rayleigh scattering. Increasing the aerosol loading from AOT_{550} = 0.10 to 0.50 substantially reduces the magnitude of the negative spectral slope because aerosol scattering has a weaker spectral dependence than molecular scattering. The presence of clouds further modifies the spectral slope, with both the thin- and thick-cloud cases generally producing substantially less negative values of m_{atm} than the cloud-free cases. The magnitude and SZA dependence of this response vary among wavelength pairs, reflecting differences in the relative contributions of aerosol and cloud scattering at the respective wavelengths.

Importantly, the simulations show that the four atmospheric cases occupy distinctly different ranges of m_{atm} over much of the investigated SZA range. In particular, the cloudy cases exhibit considerably weaker spectral dependence than the clean cloud-free case, while the polluted cloud-free atmosphere generally lies between the clean and cloudy regimes. These results demonstrate that m_{atm} is physically sensitive to changes in atmospheric scattering associated with cloud contamination and therefore provide theoretical support for the proposed cloud-screening method.

Taking this valuable comment into account, we substantially revised the methodology and updated the figures and the Results and Discussion throughout the revised manuscript by using the atmospheric spectral slope, m_{atm}, instead of the observed spectral slope, m_{obs}, derived directly from the measured detector signals. We further discussed about the results of radiative transfer calculation to demonstrate the theoritical ground of methodology in the revised manuscript (**Page 7, Lines 268- Page 8, Line 304**). As a result, the revision provides a more physically consistent interpretation of the spectral behavior by accounting for the wavelength-dependent instrumental contribution and thereby isolating the atmospheric contribution to the spectral slope. Although the revision changes the quantitative values and physical interpretation of m_{atm}, the principal findings and overall conclusion of the study remain unchanged.

(2) What is the unit of TN, FP, TP in Eqs. (3), (4), and (5)?

→ They are counts of classification outcomes, which are dimensionless. We have clarified in the revised manuscript (**Page 13, Lines 439–440**).

(3) Please explain the cloud screening method of SR-CERES. As the referees commented, in addition to the comparison with the SR-CERES method, it will be useful for the research

community to see some quantitative comparison of the present cloud screening performance and those of other methods such as Khatri and Takamura (2009).

→ In the revised manuscript, we have added a detailed explanation of the cloud screening method inlcuded in SR-CEReS package **(Page 19, Lines 608–615)**. In addition, following the reviewers' suggestions, we have carefully revised the manuscript to include a comparison of the proposed cloud screening method with existing approaches, including the method of Khatri and Takamura (2009), as detailed in Section 4.3 in the revised mansucript. The corresponding revisions and detailed responses to each reviewer comment are provided in seprate response sheets to the reviewers.

References

Gueymard, C. A.: The Sun's total and spectral irradiance for solar energy applications and solar radiation models, *Sol. Energy*, **76**, 423–453, https://doi.org/10.1016/j.solener.2003.08.039, 2004.

Khatri, P. and Takamura, T.: An algorithm to screen cloud-affected data for sky radiometer data analysis, Journal of the Meteorological Society of Japan, 87, 189–204, https://doi.org/10.2151/jmsj.87.189, 2009.

Ricchiazzi, P., Yang, S., Gautier, C., and Sowle, D.: SBDART: A Research and Teaching Software Tool for Plane-Parallel Radiative Transfer in the Earth's Atmosphere, *Bulletin of the American Meteorological Society*, **79**(10), 2101–2114, DOI: 10.1175/1520-0477(1998)079<2101:SARATS>2.0.CO;2,1998.